Optics Letters

# Spectroscopic microscopy can quantify the statistics of subdiffractional refractive-index fluctuations in media with random rough surfaces

Di Zhang,[1] Lusik Cherkezyan,[1] Ilker Capoglu,[1] Hariharan Subramanian,[1] John Chandler,[1] Sebastian Thompson,[1] Allen Taflove,[2] and Vadim Backman[1,*]

[1]Department of Biomedical Engineering, Northwestern University, Evanston, Illinois 60208, USA
[2]Department of Electrical Engineering and Computer Science, Northwestern University, Evanston, Illinois 60208, USA
*Corresponding author: v_backman@northwestern.edu

Received 17 July 2015; revised 28 September 2015; accepted 29 September 2015; posted 30 September 2015 (Doc. ID 245507); published 21 October 2015

**We previously established that spectroscopic microscopy can quantify subdiffraction-scale refractive index (RI) fluctuations in a label-free dielectric medium with a smooth surface. However, to study more realistic samples, such as biological cells, the effect of rough surface should be considered. In this Letter, we first report an analytical theory to synthesize microscopic images of a rough surface, validate this theory by finite-difference time-domain (FDTD) solutions of Maxwell's equations, and characterize the spectral properties of light reflected from a rough surface. Then, we report a technique to quantify the RI fluctuations beneath a rough surface and demonstrate its efficacy on FDTD-synthesized spectroscopic microscopy images, as well as experimental data obtained from biological cells.** 

***OCIS codes:*** (180.0180) Microscopy; (290.0290) Scattering; (300.0300) Spectroscopy; (170.1530) Cell analysis.

http://dx.doi.org/10.1364/OL.40.004931

We have previously established that, despite the fundamental diffraction limit of optical microscopy, three-dimensional subdiffraction-scale refractive-index (RI) fluctuations internal to a linear, label-free, weakly scattered dielectric medium can be detected in the far zone with spectroscopic microscopy [1]. The light scattered from RI fluctuations within an inhomogeneous sample interferes with a strong reflection from the air-sample interface, and the resulting interferogram is recorded. The expected value of intensity variance $\tilde{\Sigma}^2$ in the spectral domain of acquired images quantifies the statistics of RI fluctuations and senses structures at any length scale, limited only by the signal-to-noise ratio [2]. Thus, $\tilde{\Sigma}^2$ can quantify the subdiffractional structures in biological cells (macromolecular complexes and organelles) that were previously inaccessible using conventional microscopy and spectroscopy techniques.

In our previous work [1,2], we have shown that $\tilde{\Sigma}^2$ quantifies internal structure within an inhomogeneous sample with a flat surface. However, in most practical cases the sample surface is not flat. In case of rough surface, the information about a sample's internal structure contained in its reflected-light spectral signature is confounded by the spectrum of the light reflected from its rough surface (which serves as the reference wave). Hence, the effectiveness of detecting internal RI fluctuations could be limited by the sample's surface roughness.

Although light scattering from rough surfaces has been investigated [3,4], the spectral characteristics of rough surface reflectance at a far-field image plane have not been well described. Here, we investigate how random nanoscale height variations of the sample impact the ability of spectroscopic microscopy to quantify the RI fluctuations beneath the surface. We develop a new method of signal analysis that allows measuring RI fluctuations internal to rough samples.

This Letter is presented in the following order: (1) a theoretical foundation used to synthesize spectroscopic microscope images of rough surfaces is introduced and rigorously validated by finite-difference time-domain (FDTD) computational solutions of Maxwell's equations [5]; (2) the spectral signature of surface roughness is characterized by analyzing synthesized spectroscopic microscope images of rough surfaces with a range of roughness levels; (3) a method to measure internal RI fluctuations for media having rough surfaces is proposed; and (4) its performance is tested using FDTD simulations as well as experimental data from human buccal mucosa cells.

We first represent the sample as a homogenous dielectric medium having a refractive index $n$ and a rough surface with random height variations. For simplicity, the spatial correlation of height variations is described by an exponential function:

$$B_h(r) = \sigma_h^2 e^{-r/lc_h}, \tag{1}$$

where $r$ represents the radial distance along the x–y plane and $h$ represents the height. The statistics of surface roughness can be characterized by two parameters: the height variance $\sigma_h^2$ and correlation length $lc_h$.

0146-9592/15/214931-04$15/0$15.00 

Corrected 3 November 2015

Figure 1 illustrates an example of a rough surface having random height variations generated using MATLAB. An x-polarized plane wave with wavenumber $\boldsymbol{k}_i$ and electric field vector $\boldsymbol{E}_i$ impinges on the rough surface from free space and is scattered. The scattered light propagates along $\boldsymbol{k}_s$ at angle $(\theta, \phi)$ with an electric field vector $\boldsymbol{E}_s$ perpendicular to $\boldsymbol{k}_s$. $\boldsymbol{k}_i$ and $\boldsymbol{k}_s$ form the scattering plane. $\boldsymbol{E}_s$ can be decomposed to $E_\theta$ (parallel to the scattering plane) and $E_\phi$ (perpendicular to the scattering plane).

Next, we assess the scattering amplitude by Kirchhoff approximation (KA). KA was initially used to describe scattering from surfaces with large length scales ($lc_s > \lambda$) [4], but has been extended to dielectrics with subdiffractional scales ($lc_s < \lambda$) [6]. The validity of KA is dependent on $n$, $\sigma_h$, $lc_h$, and the angles of illumination and observation [6]. Thus, it is unclear whether KA applies to the present circumstances ($n = 1.53$, $\sigma_h = 10$–$50$ nm, and $lc_h = 60$–$240$ cm). The ranges of $\sigma_h$ and $lc_h$ were selected to include (but not be limited to) those of human buccal mucosa cells, as measured by atomic force microscopy (AFM). Referring to Chapter 3 of [3], we note that the scattered electric field in the far zone can be calculated as

$$E_\theta = \frac{A \sin\varphi}{k}\left(\frac{2\cos\theta + 1}{2(\cos\theta + 1)}\right)\sin^2\chi F\{\Delta n(\boldsymbol{r})\},$$
$$E_\phi = \frac{A \cos\varphi}{k}\left(\frac{1}{2(\cos\theta + 1)}\right)\sin^2\chi F\{\Delta n(\boldsymbol{r})\}, \quad \textbf{(2)}$$

where $A = -\pi|\boldsymbol{E}_i|\ln n$ is a constant, $k$ represents the wavenumber in vacuum, $\sin^2\chi = 1 - \sin^2\theta\cos^2\phi$ is the polarization factor, and $F$ and $\Delta$ represent the Fourier transform and the Laplacian operators, respectively. $n(\boldsymbol{r})$ equals $n$ below the surface and $n_0$ above the surface.

The scattered field is then focused onto an image plane with a moderate numerical aperture (NA) of 0.6 [7]:

$$\boldsymbol{E}_{\text{img}}(x', y', k) = \frac{ik}{2\pi}\iint_{\Omega_{\text{img}}} \boldsymbol{E}_s(s_x, s_y, k)e^{-ik(s_x x' + s_y y')}\,d\Omega, \quad \textbf{(3)}$$

where $\boldsymbol{E}_{\text{img}}$ represents the field at the image plane $(x', y')$ with wavenumber $k$ in the vacuum, $\Omega_{\text{img}}$ represents the solid angle limited by the NA, and $s_x$ and $s_y$ are the direction cosines $(s_x, s_y) = (\cos\phi\sin\theta, \sin\phi\sin\theta)$. The image of the rough surface $I_h(x', y', k) = |E_{\text{img}}(x', y', k)|^2$ is normalized by that of a smooth surface with the same RI, i.e., by intensity in the absence of roughness.

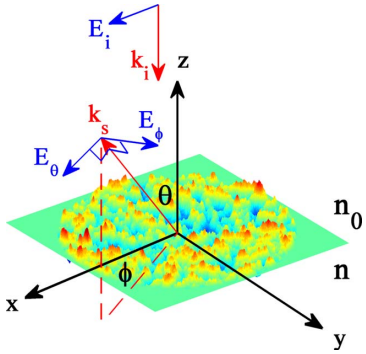


**Fig. 1.** Geometry of a rough surface.

To validate that KA applies to the selected roughness levels, we compared KA-predicted spectroscopic microscope images with those synthesized by FDTD solutions of Maxwell's equations. FDTD simulations were performed using Angora [8], an open-source FDTD software package developed in our lab.

We establish that, for all tested levels of surface roughness, the KA-synthesized microscope images agreed very well with those synthesized by FDTD, with coefficients of determination ($R^2$) exceeding 0.8. Figures 2(a)–2(d) illustrate the high level of agreement ($R^2 = 0.92$) of the FDTD- and KA-synthesized grayscale microscope images of a rough surface ($\sigma_h = 35$ nm, $lc_h = 170$ nm). Moreover, an excellent pixel-specific match is observed between wavelength-dependent spectra of rough surface reflectance predicted by FDTD and KA [as illustrated in Fig. 2(f)].

To study the spectral signature of the rough surface reflectance, we average the image spectra $I_h(x', y', k)$ over the surface area and multiple samples to obtain a unique characteristic spectrum (mean spectrum) for each combination of $\sigma_h$ and $lc_h$ [Fig. 3(c)]. By analyzing the mean spectra, we observed that, regardless of surface roughness levels, the intensity decreases with $k$ [Figs. 3(a) and 3(b)]. Further, we compared the Fourier transform of $I_h(x', y', k)$ with that of $I_n(x', y', k)$, the reflectance spectrum from a smooth inhomogeneous sample. We find that $F_k\{I_h(x', y', k)\}$ contains predominantly low-frequency components and rapidly decays at higher frequencies, while $F_k\{I_n(x', y', k)\}$ is distributed along all frequencies

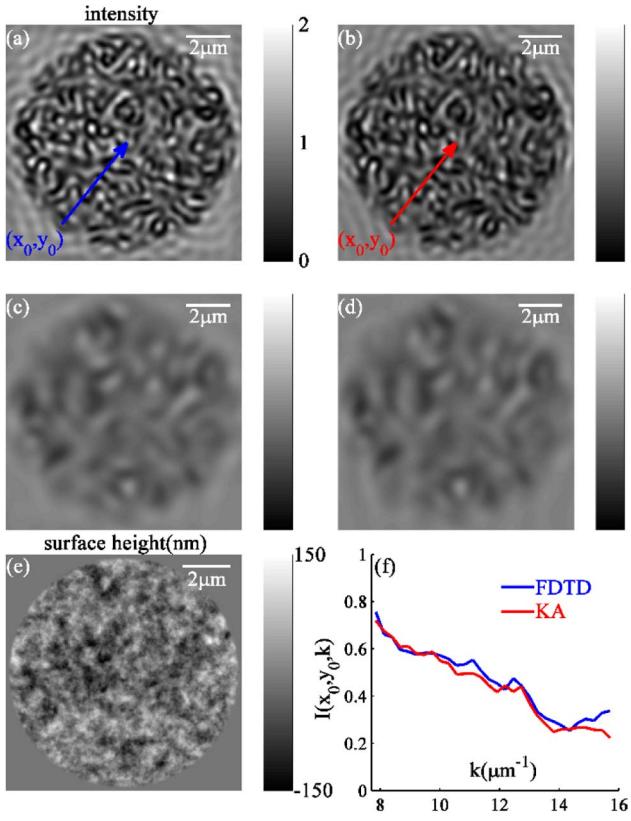


**Fig. 2.** Comparisons of (a), (c) FDTD-synthesized and (b), (d) KA-synthesized microscope images of a rough surface with $\sigma_h = 35$ nm and $lc_h = 170$ nm: $\lambda = 400$ nm for (a) and (b); $\lambda = 800$ nm for (c) and (d). (e) Height map of the same surface. (f) Comparative FDTD- and KA-synthesized center pixel $(x_0, y_0)$ spectra.

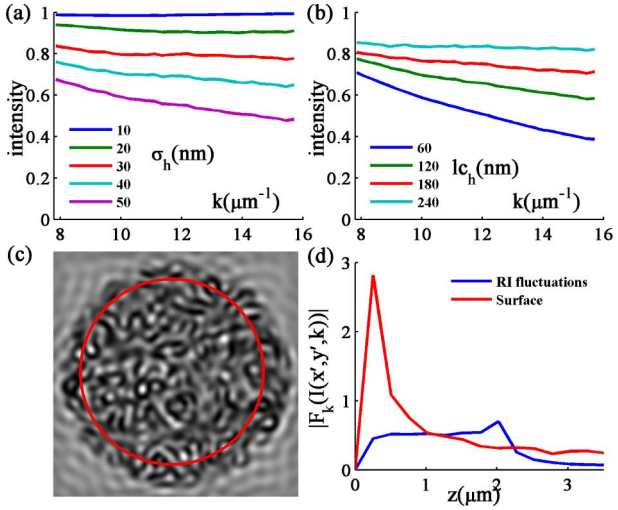


**Fig. 3.** (a) Mean spectra for a fixed $lc_h$ of 150 nm and $\sigma_h$ from 10–50 nm. (b) Mean spectra for a fixed $\sigma_h$ of 35 nm and $lc_h$ from 60–240 nm. (c) Mean spectra are calculated by averaging over pixels in the red circle and further averaging over 10 samples. (d) Averaged Fourier transforms of $I_h(x', y', k)$ (surface) and $I_n(x', y', k)$ (RI fluctuations). The frequencies of spectra are translated into the depths from surface.

bounded by the thickness of the sample [Fig. 3(d)]. Analysis of these spectral characteristics of surface roughness establishes the foundation for the development of techniques to measure internal RI fluctuations in media having rough surfaces.

We next consider the case where a sample has RI fluctuations underlying a rough surface. The internal RI fluctuations have an exponential form of spatial correlation function, described by the correlation length $lc_n$ and variance $\sigma_n^2$. Our goal is to extract the spectral variance component that describes the internal RI fluctuations ($\Sigma_n^2$) from the wavelength-resolved microscope image of the sample $I(x', y', k)$. By estimating $\Sigma_n^2$, we can quantify the statistics of RI fluctuations at the nanoscale. For clarity, we denote $\tilde{\Sigma}^2$ to represent the expected value of spectral variance directly measured from $I(x', y', k)$ and $\Sigma_n'^2$ to represent the estimation of $\Sigma_n^2$ from samples having rough surfaces.

We first present analytical equations to represent $I(x', y', k)$ reflected from an inhomogeneous sample with smooth and rough surfaces. Ignoring the energy loss during light transmitting through the top surface of the sample, the microscope image intensity for a random media with a smooth surface can be expressed as

$$I(x', y', k) = \Gamma_{01}^2 - 2\Gamma_{01}\,\mathrm{Im}\left\{\int_{-\infty}^{+\infty} k n_{1D}(\boldsymbol{r}) e^{-i2kz} dz\right\}, \quad (4)$$

where $\Gamma_{01}$ is the amplitude Fresnel reflectance coefficient and Im denotes "the imaginary part of." $n_{1D}(\boldsymbol{r})$ denotes $n_\Delta(\boldsymbol{r})$ (zero-mean RI fluctuations normalized by the average $n$) convolved with the point spread function of the microscope. The expected value of the recorded spectral variance is proportional to $\Sigma_n^2$. For smooth surfaces, $\tilde{\Sigma}^2 = \Sigma_n^2$.

In the case when the surface of the inhomogeneous sample is rough, the reflectance from the air-sample interface becomes wavelength- and position-dependent. Therefore, the image intensity becomes

$$I(x', y', k) = \Gamma_{01}^2 I_s(x', y', k) - 2\Gamma_{01}\sqrt{I_s(x', y', k)} \times \mathrm{Im}\left\{\int_{-\infty}^{+\infty} k n_{1D}(r) e^{-i2kz} dz\right\}. \quad (5)$$

By analyzing (5), one sees that, in order to obtain $\Sigma_n^2$, we must acquire $I_s(x', y', k)$ first. With a known surface profile, $I_s(x', y', k)$ can be accurately determined by KA or FDTD. Without surface information, one should seek a signal processing approach to estimate $I_s(x', y', k)$ from $I(x', y', k)$. Based on our previous analysis, the first term on the right-hand side contains predominantly low-frequency components. The second term is an interference term that has higher frequency components, multiplied by $\sqrt{I_s(x', y', k)}$. Therefore, it is possible to separate $I_s(x', y', k)$ by fitting $I(x', y', k)$ with low-frequency functions at each individual pixel $(x', y')$. Here, we propose to use second-order polynomial fitting to acquire $I_s(x', y', k)$. Once $I_s(x', y', k)$ is obtained, $\Sigma_n^2$ may be readily estimated from Eq. (5).

We then evaluate the efficacy of the proposed method via a challenge to distinguish samples with different $lc_n$ and the same surface profile. The test was performed in the following sequence. First, 2 μm thick inhomogeneous media with smooth surfaces were generated numerically with $\sigma_n = 0.033$, and $lc_n = 20$ nm for one group ($N = 10$) and 100 nm for another ($N = 10$). FDTD simulations were performed to obtain the spectroscopic microscopic images. For each group, $\Sigma_n^2$ was calculated and averaged over 25 pixels per sample and 10 samples per group. This is the spectral variance caused only by RI fluctuations (no influence from the rough surface), and the difference of $\Sigma_n^2$ between $lc_n$ of 20 and 100 nm represents the baseline for the power of spectroscopic microscopy to distinguish different $lc_n$. As expected, $\Sigma_n$ of $lc_n$ 100 nm is significantly higher than that of 20 nm [Fig. 4(b), $p < 0.001$].

Thereafter, the same media were generated with rough surfaces ($\sigma_h = 35$ nm and $lc_h = 170$ nm). FDTD simulations were performed to obtain the spectroscopic microscopic images, and $\tilde{\Sigma}^2$ and $\Sigma_n'^2$ were calculated. Figure 4(a) illustrates second-order polynomial fits to image spectra from inhomogeneous media having smooth and rough surfaces. The results showed that the proposed method ($\Sigma_n'$) allowed the difference in internal structure to be identified [Fig. 4(c), $p < 0.001$]. Note that this approach did not disturb the ability of distinguishing different $lc_n$ for media with smooth surfaces [Fig. 4(b), $p < 0.001$]. Moreover, $\Sigma_n'$ were close to $\Sigma_n$ [Figs. 4(b) and 4(c)] with acceptable error (11% for $lc_n$ of 20 nm and 7% for 100 nm).

We further investigated the validity of the proposed approach by evaluating $\Sigma_n'^2$ from homogenous samples having rough surfaces ($\Sigma_n^2 = 0$). Using the FDTD, we found that, for $\lambda = 500$–$700$ nm, NA = 0.6, and sample thickness $L > 0.8$ μm, the proposed method holds for a wide range of parameters: $\sigma_h = 10$–$35$ nm, $lc_h = 60$–$240$ nm, $\sigma_n > 0.03$, and $lc_n > 20$ nm.

Lastly, we illustrate the efficacy of the proposed method experimentally by identifying nanoscale structural alterations within human buccal mucosa cells during development of lung cancer. Histologically (microscopically) normal buccal epithelium is known to undergo genetic and epigenetic alterations during the progression of lung cancer [9]. This implies that the buccal nanoscale organization in lung cancer patients may be distinct from that of healthy individuals. Herein, we use

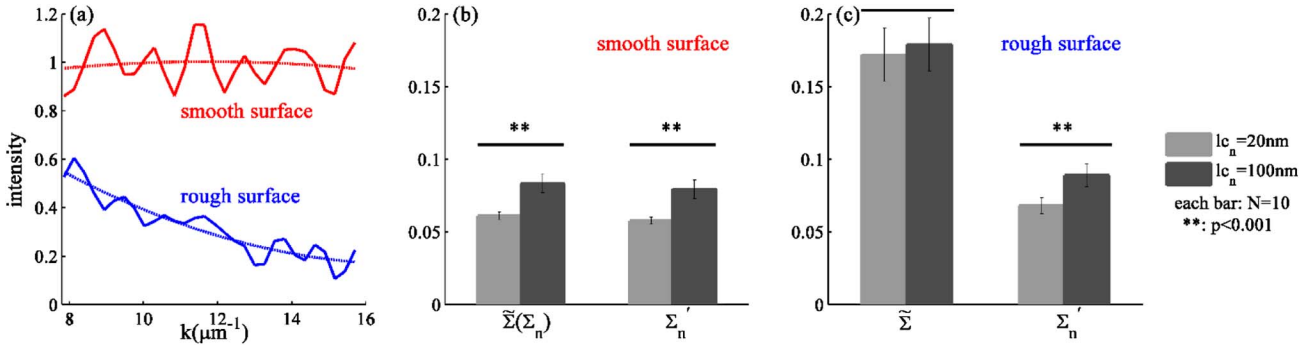


**Fig. 4.** (a) Example of image spectra from the same pixel of the same medium having smooth and rough surfaces. The dash lines represent second-order polynomial fits for $I_s(x', y', k)$; comparison of estimated $\Sigma_n$ from inhomogeneous media with $lc_n$ of 20 and 100 nm, calculated from sample with smooth surfaces (b) or rough surfaces (c), without ($\tilde{\Sigma}$) or with ($\Sigma_n'$) second-order polynomial fitting.

spectroscopic microscopy, followed by the spectral analysis method developed above, to quantify and compare the nanoscale structure within buccal cells of patients with and without lung cancer. AFM measurements on these fixed buccal cells revealed that L = 0.8–1.5 um, $\sigma_b = 19.7 \pm 5.1$ nm, and $lc_b = 167 \pm 36$ nm. $\sigma_n$ of biological tissue is estimated 0.04–0.10 [10]. Similarly, after collecting spectroscopic microscopy images from 23 patient samples (30 cells each), $\tilde{\Sigma}$ and $\Sigma_n'$ were calculated. Our results showed that the recorded spectral variance by itself is identical between the two groups. However, when the spectral contribution from the sample's surface roughness is removed, a significant difference in the buccal intracellular nanoscale structures between patients with and without lung cancer is revealed ($\Sigma_n'$, $p < 0.01$, Fig. 5).

We conclude that the second-order polynomial fitting method accurately separates the spectral variance component caused by internal RI fluctuations from that caused by the rough surface. We demonstrate that $\Sigma_n'^2$ is a roughness-independent measurement of RI fluctuations within an inhomogeneous sample, which was validated by FDTD for all roughness levels tested (including smooth surface).

In this Letter, we validated the precision of KA for modeling light scattering from rough surfaces of biological cells. With the characteristic mean spectra obtained from spectroscopic microscopic images of homogenous samples having rough surfaces, we described the signature of surface roughness on the spectral component of microscopic images. Furthermore, we developed a method for detecting RI fluctuations in media with rough surfaces. This Letter enables spectroscopic microscopy measurement of nanoarchitectural alterations beneath rough surfaces in biological cells, leading to more accurate identification of multiple human cancers.

The analysis and technique reported in this Letter have two primary limitations. First, the autocorrelation of the random surface was modeled as exponential. It is possible that surfaces of biological cells have different types of autocorrelation functions. Second, the accuracy of predicting $\Sigma_n^2$ relies upon an appropriate fitting for $I_s(x', y', k)$. Although second-order polynomial fitting was demonstrated to have considerable accuracy, there may be more accurate methods. Potential alternatives include various types of filters and windows.

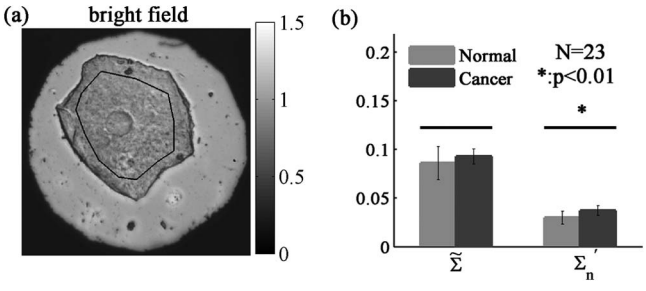


**Fig. 5.** (a) Example of bright field reflectance image of a human buccal mucosa cell. (b) Performance of $\tilde{\Sigma}$ and $\Sigma_n'$ in distinguishing the buccal intracellular structure between patients with and without lung cancer. The outline within the cell in (a) indicates the region of interest.

**Funding.** National Institutes of Health (NIH) (R01CA155284, R01CA165309, R01EB016983); National Science Foundation (NSF) (EFRI-1240416).

**Acknowledgment.** The FDTD simulations were made possible by a computational allocation from the Quest high performance computing facility at Northwestern University.

## REFERENCES

1. L. Cherkezyan, I. Capoglu, H. Subramanian, J. D. Rogers, D. Damania, A. Taflove, and V. Backman, Phys. Rev. Lett. **111**, 033903 (2013).
2. L. Cherkezyan, H. Subramanian, and V. Backman, Opt. Lett. **39**, 4290 (2014).
3. A. A. Maradudin, *Light Scattering and Nanoscale Surface Roughness* (Springer, 2007).
4. P. Beckmann and A. Spizzichino, *The Scattering of Electromagnetic Waves from Rough Surfaces* (Macmillan, 1963).
5. A. Taflove and S. C. Hagness, *Computational Electrodynamics: The Finite-Difference Time-Domain Method*, 3rd ed. (Artech, 2005).
6. J. A. Sanchez-Gil and M. Nieto-Vesperinas, J. Opt. Soc. Am. A **8**, 1270 (1991).
7. J. Goodman, *Introduction To Fourier Optics*, McGraw-Hill Physical and Quantum Electronics Series (Roberts, 2005), pp. 126–154.
8. I. R. Capoglu, "ANGORA: A free software package for finite-difference time-domain (FDTD) electromagnetic simulation" (2012), date accessed: April 2012, http://www.angorafdtd.org.
9. K. Steiling, J. Ryan, J. S. Brody, and A. Spira, Cancer Prev. Res. **1**, 396 (2008).
10. J. M. Schmitt and G. Kumar, Appl. Opt. **37**, 2788 (1998).